

Agile and Energy-Efficient Jumping–Crawling Robot Through Rapid Transition of Locomotion and Enhanced Jumping Height Adjustment

Soo-Hwan Chae , Student Member, IEEE, Sang-Min Baek , Jongeun Lee , and Kyu-Jin Cho , Member, IEEE

Abstract—A small-scale jumping–crawling robot expands the accessible region of a robot by selectively performing suitable locomotion type. However, the parallel elastic actuation for jumping, which amplifies a lightweight actuator’s limited power, couples the motion between the energy storing process and the crouching of the jumping linkage. This coupling hinders the quick transition of the locomotion from jumping to crawling and limits the jumping height control. Furthermore, these two defects degrade the agility and the energy-efficiency of the robot. In this article, we present a jumping–crawling robot with enhanced agility and energy-efficiency by decoupling the energy storage and crouching of the jumping linkage. The decoupling is achieved by implementing a passive clutch that properly switches the connection between the energy storage component and the jumping linkage. As a result, the proposed jumping–crawling robot can promptly change the locomotion type, and can adjust the jumping height from 0.1 to 0.8 m. These features reduce the time and energy consumption of the jumping–crawling robot during the demonstration of multimodal locomotion up to 40 and 30% respectively, compared to the robot without the proposed decoupling approach.

Index Terms—Jumping–crawling robot, mobile robot, multimodal locomotion.

I. INTRODUCTION

SMALL creatures in nature perform specialized locomotion to adaptively move on uneven terrain or escape from predators [1]. Inspired by these creatures, centimeter-scale locomotive robots have been developed, such as crawling robots [2]–[13], climbing robots [14], [15], jumping robots [16]–[19], and flying robots [20]–[24], to navigate unstructured environments [25];

Manuscript received 25 May 2022; accepted 26 June 2022. Recommended by Technical Editor F. Auat Cheein and Senior Editor W. J. C. Zhang. This work was supported in part by the grant to Bio-Mimetic Robot Research Center Funded by Defense Acquisition Program Administration and in part by the Agency for Defense Development (UD190018ID). (Corresponding author: Kyu-Jin Cho.)

The authors are with the Biorobotics Laboratory, Department of Mechanical Engineering, IAMD, Seoul National University, Seoul 08826, South Korea (e-mail: justices@snu.ac.kr; bsm6656@snu.ac.kr; yhjelee@snu.ac.kr; kjcho@snu.ac.kr).

This article has supplementary material provided by the authors and color versions of one or more figures available at <https://doi.org/10.1109/TMECH.2022.3190673>.

Digital Object Identifier 10.1109/TMECH.2022.3190673

these robots can assist or replace humans in accomplishing tasks, such as search and rescue missions in disaster areas. Moreover, by combining two or more different locomotive mechanisms, multimodal locomotive robots have been developed, such as jumping–crawling [26]–[32], crawling–flying [33], [34], crawling–gliding [35], jumping–gliding [35]–[37], and flying–climbing [38] robots. Multimodal robots can selectively perform locomotion suitable for various environments, reducing the cost of transport and widening the regions accessible to these robots [39].

In particular, a jumping–crawling robot has the ability to rapidly and efficiently overcome various sizes of ground obstacles. By crawling, the robot can rapidly traverse a bumpy field, which consists of a series of relatively small obstacles [2]–[13]. A terrestrial locomotive robot usually encounters these kinds of fields, including grasslands and gravel roads, and can proceed until it faces an obstacle larger than the robot. By jumping, the robot can cross large obstacles ballistically. To propel itself, the robot should apply a large impulsive force (i.e., large power) to the ground. Usually, the power of the actuator used in a centimeter-scale robot is far less than the power required for jumping [40]. Therefore, an energy storage component, such as a spring, is required to amplify the output power [16]–[19]. As the actuator slowly deforms the spring, elastic potential energy is accumulated. Subsequently, all the stored potential energy in the spring is suddenly released and converted to the kinetic energy of the robot through a jumping linkage, where the spring is directly attached; recoil of the spring derives a vertical movement of the jumping linkage from crouching to extending, generating an impulsive ground reaction force (GRF) for jumping. The accessible region of the robot is expanded by strategically performing jumping or crawling depending on the encountered obstacles.

Prior research efforts mainly focused on enhancing the performance of individual locomotion type (see Table I). For example, the MSU jump-runner [31] reduces the robot’s mass to increase the jumping height. The Mini-Whegs 9J [26] uses a legged-wheel to increase the crawling speed. The surveillance robot [32] increased energy-efficiency by adjusting the take-off angle. JumpRoACH [28] shows a slight ability of jumping height adjusting but mostly focused on the energy storage maximization to increase the jumping height. However, all previously developed jumping–crawling robots have two limitations that hinder their

TABLE I
COMPARISON OF JUMPING–CRAWLING ROBOTS

<i>Jumping-Crawling robot</i>	<i>Size (cm)</i>	<i>Mass (g)</i>	<i>Jumping height (m)</i>	<i>Crawling Speed (m/s)</i>	<i>Jumping Linkage and the Spring</i>	<i>Transition duration* (s)</i>	<i>Adjustable range of jumping height (h/h_{max})</i>
Scout [26]	11.5	200	0.57	N/A	Attached	63	Fixed
Mini-Whegs 9j [27]	12	191	0.18	0.3	Attached	N/A	Fixed
JumpRoACH [28]	12	99	1.5	0.56	Attached	68	0.7 – 1
One-motor driven robot [29]	10	52	0.33	0.0014	Attached	46	Fixed
Locust-inspired robot[30]	8	6	0.02	0.082	Attached	10	Fixed
MSU jump-runner [31]	9	25	1.43	0.05	Attached	10	Fixed
Surveillance Robot [32]	14	250	0.41	0.04	Attached	15	0.5 – 1
Proposed robot	10	105	0.8	0.67	Partially detached	0	0.125 – 1

* Transition duration was measured from the moment finishing the one locomotion type, to the moment the other locomotive mechanism contacting with the ground to ready to start the other locomotion type.

agility and energy efficiency. The agility and energy-efficiency determine how fast the robot can complete the mission and how long the robot can be operated. Two limitations that hinder the agility and energy-efficiency are as follows: 1) the robot consumes tens of seconds to change their locomotion type, and 2) the jumping height adjustment range is limited (see Table I). These limitations are related to the interaction between the two different locomotive mechanisms caused by integrating them into a single robot, which has not been studied previously.

In a multimodal robot, since two different locomotive mechanisms are integrated into a single body, the movements of two mechanisms can physically interfere with each other. In the case of jumping–crawling robots, since both locomotion types are terrestrial movements, each locomotive mechanism must be in contact with the ground during the locomotion to get the proper GRF. Because the required force of each locomotion type is different, contact with the ground of one locomotive mechanism generates the force that disturbs the other performing locomotion. Thus, it is efficient that the resting mechanism should not be in contact with the ground during performing the other locomotion. During crawling, the resting jumping linkage should be crouched and placed above the crawling linkage, in order for it not to contact the ground. Otherwise, during jumping, the jumping linkage should be extended below the crawling linkage to contact the ground. Therefore, the crouching and extending movement of the jumping linkage plays an important role in the transition of locomotion by determining which mechanism is in contact with the ground. Additionally, as shown in Table I, the spring is attached to the jumping linkage, which makes the movement of the jumping linkage play another important role: the control of the elastic energy storage. Since two different roles are embodied in the movement of the jumping linkage, transition of locomotion and control of the energy storage are coupled, provoking the two limitations mentioned above. In order to change the locomotion type, energy should be stored in the spring, which requires lots of time. Moreover, it is hard to control the amount of energy storage after the type of locomotion is changed.

In this article, we propose an agile and energy-efficient jumping–crawling robot through the rapid transition of locomotion and enhanced jumping height adjustment (see Fig. 1). These advances are accomplished by decoupling the movement

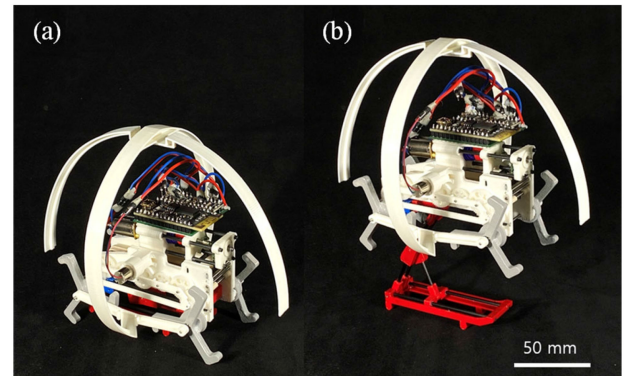


Fig. 1. Agile and energy-efficient jumping–crawling robot with (a) crouched and (b) extended jumping linkage.

of the jumping linkage and control of the energy storage of the robot. To decouple the movement of the jumping linkage and the control of the energy storage, we developed a passive clutch for a jumping mechanism that switches the connection between the linkage and the spring depending on the operating state. When preparing for jumping, the linkage and the spring are disconnected; thus, the linkage can be crouched without storing the energy in the spring, and energy storage can be controlled by deforming the spring while maintaining the crouched jumping linkage. When jumping is started, the linkage and spring are connected by the clutch, so the stored energy in the spring is released through the extending jumping linkage, and is converted to the kinetic energy of the robot. By employing the decoupling clutch, the jumping–crawling robot can crawl right after jumping, and can adjust the jumping height from 0.1 to 0.8 m. To validate the enhanced performance, we conducted a demonstration of multimodal locomotion, which shows a reduction of the time and energy consumption of the jumping–crawling robot up to 40% and 30% respectively, compared to the robot without the proposed decoupling mechanism. Further from the mechanism point of enhancement, this result shows our decoupling approach is feasible for increasing the agility and energy-efficiency of a jumping–crawling robot, and this approach can be applied to different types of jumping–crawling robots that use parallel elastic systems to enhance performances.

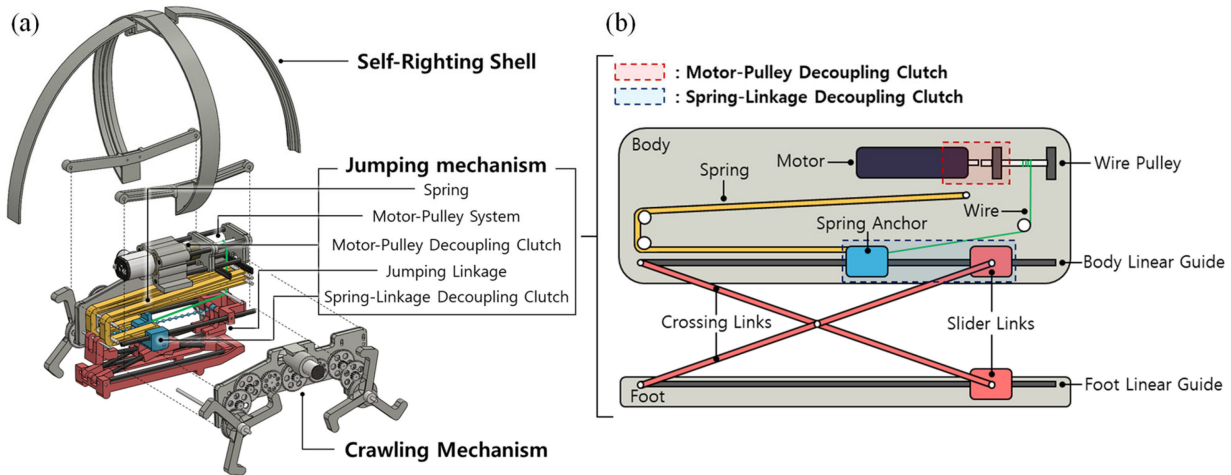


Fig. 2. (a) Exploded view of the proposed jumping–crawling robot. The robot consists of a jumping mechanism, a crawling mechanism, and a self-righting shell. (b) Schematic of the jumping mechanism. The jumping mechanism consists of the body, spring, motor–pulley system, jumping linkage, motor–pulley decoupling clutch for switching the connection between the motor and a wire pulley, and a spring-linkage decoupling clutch for switching the connection between the spring and the linkage.

The rest of this article is organized as follows. The overall design of the proposed jumping–crawling robot is explained in Section II. Section III introduces quasi-static models of the clutch design, and a dynamic jumping model that predicts the jumping height. Experiments and demonstration to validate the performance of the proposed robot are described in Section IV. Finally, Section V concludes this article.

II. ROBOT DESIGN

The proposed jumping–crawling robot consists of a jumping mechanism, a crawling mechanism, and a self-righting shell as shown in Fig. 2(a). Specifically, the jumping mechanism consists of a spring for the energy storage component, a motor–pulley system for deforming the spring to store the elastic energy, and a motor–pulley decoupling clutch for switching the connection between the motor and pulley to release the stored elastic energy of the spring at once, and a jumping linkage for converting the released elastic energy into the kinetic energy of the robot. In addition, there is a spring-linkage decoupling clutch that controls the connection between the spring and the linkage to decouple the movement of the jumping linkage and the control of the energy storage.

A. Spring, Linkage, and Motor–Pulley System

Fig. 2(b) is a schematic of the jumping mechanism. A dc motor is used as an actuator to store the elastic energy in the spring. The motor can deform the spring by pulling the wire, which connects one end of the spring and a motor–pulley; the motor rotates the pulley to pull the wire. The other end of the spring is grounded to the body. A spring anchor is used for the connection part between the spring and the wire. Also, the spring anchor is connected to the linear guide as a prismatic joint, so the spring is deformed following the linear guide. A latex band was used for the spring component, which has a high energy density and low hysteresis [41], [42]. A latex spring is basically nonlinear in a

full range of elongation. However, it can be assumed as a linear spring within a limited range of elongation. We assumed the stiffness of the spring as 500 N/m; we conducted the tensile test of the spring in elongation range of our application and the result was linearly fitted by stiffness of 499.6 N/m with a coefficient of determination (R^2) of 0.9973. The spring is prestretched from a natural length of 42 mm to a length of 97 mm after being connected to the spring anchor, and it can be elongated to the maximum length of 144 mm for energy storage.

To create the vertical movement of the jumping linkage, a scissors mechanism is employed. It consists of two crossing links, two slider links, and linear guides on a body and a foot [see Fig. 2(b)]. A horizontal movement of the upper slider link on the body linear guide generates the vertical displacement between the body and foot.

B. Motor–Pulley Decoupling Active Clutch

To release all the stored energy in the spring at once, the stretched spring has to be freed from the motor. To release the spring from the motor, a motor–pulley decoupling active clutch, which switches the connection between the motor and the wire pulley, was developed. The clutch consists of a motor and its case, a wire pulley, a motor coupling gears, and a pulley coupling gears, as shown in Fig. 3(a). Of note, the lead screw and lead nut structure are embedded in the motor coupling gear and the motor case, respectively. These structures change the rotational motion of the motor axis to a linear motion of the motor itself, so the motor can move forward or backward relative to the motor case. This linear motion switches the engagement of the motor coupling gear and the pulley coupling gear.

Fig. 3(b)–(d) is a schematic of the working procedure of the clutch. If the motor rotates in the x -direction, the motor linearly moves in the x -direction and the two coupling gears are engaged [see Fig. 3(b)]. After engaging the two coupling gears, the torque of the motor is transferred to the wire pulley. At the same time,

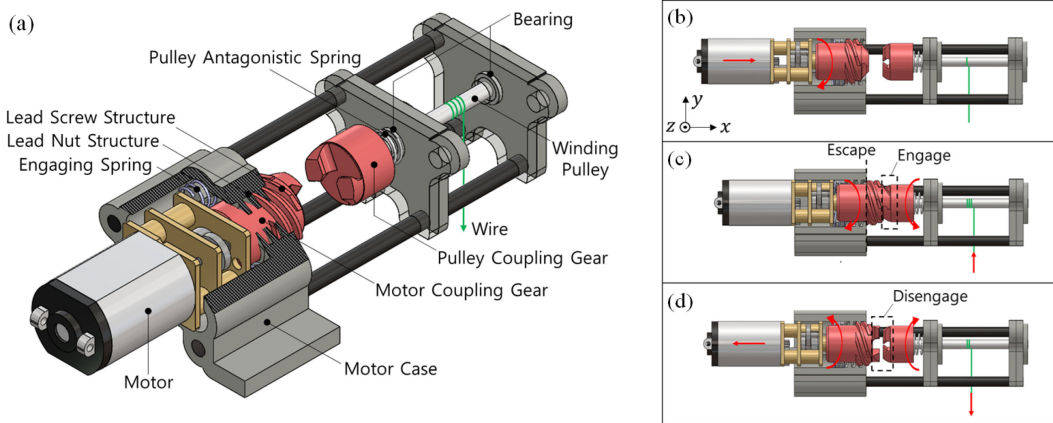


Fig. 3. (a) Schematic of the motor–pulley system and decoupling clutch. It consists of the motor, winding pulley, motor and pulley coupling gear, and motor case. Of note, the lead screw and nut structure are embedded at the motor coupling gear and motor case, respectively, converting the rotational motion to the linear motion of the motor and the coupling gear. (b) Motor moves forward when it rotates in a clockwise direction. (c) After two coupling gears are engaged, the motor transfers the torque to the winding pulley. (d) Motor moves backward when it rotates in a counter-clockwise direction. After two coupling gears are disengaged, the pulley freely rotates.

the screw structure of the motor coupling gear escapes from the nut structure of the motor case, so the motor does not move forward anymore and purely rotates to wind the pulley [see Fig. 3(c)]. If the motor rotates in the $-x$ -direction, the screw and nut structures are re-engaged with the help of the engaging spring by pushing the motor in the $-x$ -direction. After the engagement, the motor linearly moves in the $-x$ -direction and the two coupling gears are disengaged. Then, the wire pulley is released from the motor and it freely rotates [see Fig. 3(d)]. Through this clutch, the motor can pull the wire to stretch the spring to the desired length, and release the wire to recoil the spring at the desired timing.

C. Spring-Linkage Decoupling Passive Clutch

To decouple the movement of the jumping linkage and the control of the energy storage of the spring, a spring-linkage decoupling clutch was developed to passively switch the connection between the jumping linkage and the spring (see Fig. 4). When preparing for jumping, the linkage, and the spring are disconnected, the linkage is crouched without storing energy, so the energy storage can be controlled while maintaining the crouched jumping linkage. On the other hand, when jumping is started, the linkage and the spring are connected by the clutch, and the recoil force of the spring is transferred to the extending jumping linkage and to the ground. Fig 4(a) shows a schematic of the spring-linkage decoupling clutch. Knotted string is embedded into the slider link of the jumping linkage, and a clamping claw is embedded in the spring anchor; these are the key components to switch the connection between the jumping linkage and the spring. The knotted string passes through the gap between the claws, and the claws can clamp or unclamp the knotted string. If the claws clamp the knotted string, the spring anchor, and slider link are connected. Otherwise, if the claws unclamp the knotted string, they are disconnected. The clamping motion is generated by the movement of the rotational claw; the claws consist of a fixed claw embedded at the spring anchor, and

a rotational claw pin-jointed to the spring anchor. The rotation of the rotational claw opens or closes the gap where the knotted string passes through. The spring and motor wire are connected to the rotational claw, generating closing, and opening torque of the claws, respectively.

Fig. 4(b)–(g) shows the operation procedure of the clutch during storing energy and releasing energy. To store the energy, the motor pulls the wire connected to the rotational claw of the spring anchor [see Fig. 4(b)]. The spring anchor moves following the linear guide and the spring is stretched until the claws contact with the knot. The normal force of the knot generates a torque to the claws in the $-z$ -direction, which tries to open the claws. In this case, the torque of the motor wire helps to open the claws. Thus, the claws are opened [see Fig. 4(c)], so the spring anchor passes by the knotted string of the slider link [see Fig. 4(d)]; this means that the spring can be stretched to the desired length, while maintaining the crouched jumping linkage.

In the case of an energy release, as the tensed wire is released from the motor and loses its tension, the spring starts to recoil [see Fig. 4(e)]. During recoiling, the claws contact the nearest knot in the opposite direction compared to the energy-storing process, and the normal force of the knot tries to open the claws again. However, this force is not enough to open the claws, because the opening torque previously generated by the motor wire disappears. Because the knot cannot pass through the claws, the knotted string of the slider link has to move with the spring anchor [see Fig. 4(f)]; this means that the recoil force of the spring is transferred to the extending jumping linkage. After releasing the energy, the upper part of the rotational claw contacts with the decoupling pin. The decoupling pin generates a torque in the $-z$ -direction to the rotational claw which tries to open the claws. This torque is larger than the closing torque of the spring; thus, the claws open again and free the knotted string [see Fig. 4(g)]. As a result, the slider link is moved to the initial position by the attached antagonistic spring, which means that the jumping linkage is rapidly crouched without storing energy.

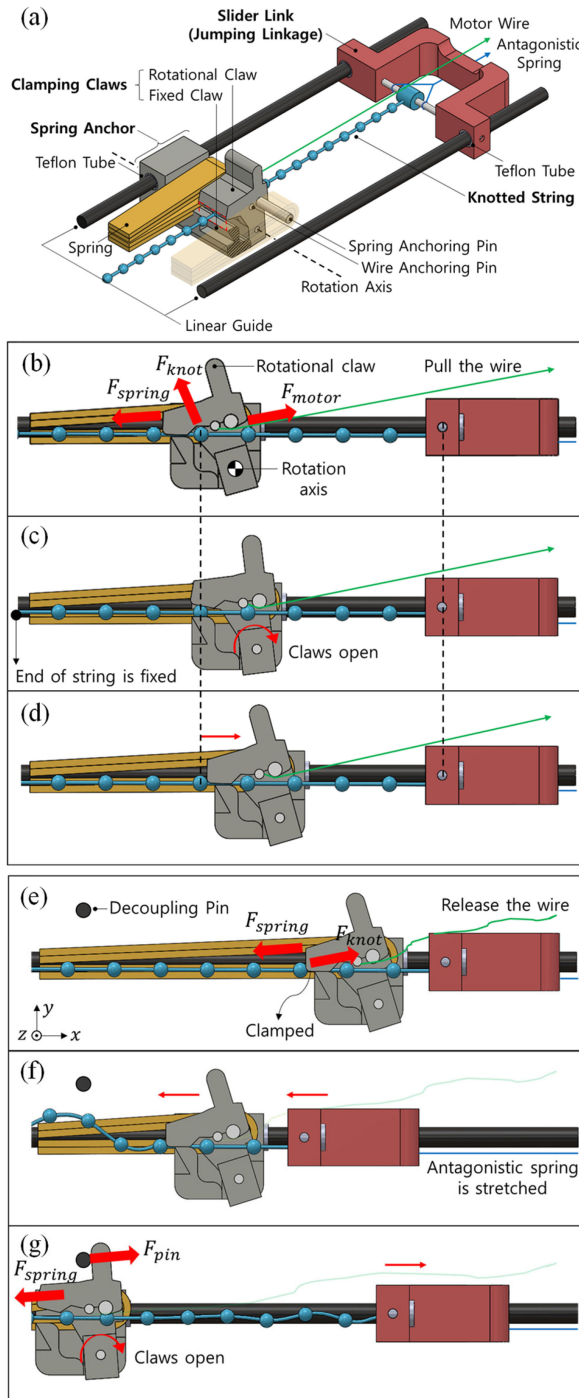


Fig. 4. (a) Schematic of the spring-linkage decoupling clutch. It consists of clamping claws embedded at the spring anchor, and a knotted string embedded in the slider link of the jumping linkage, which passes through the gap between the claws. Operation procedure of the clutch for (b)–(d) storing the energy, and (e)–(g) releasing the stored energy.

D. Crawling Mechanism

A legged-wheel mechanism is used to generate a simple and fast crawling motion, similar to that described in [27] [see Fig. 2(a)]. A total of four legged-wheels (3 spokes, radius of 2.3 cm) are connected to the body as revolute joints, and wheels

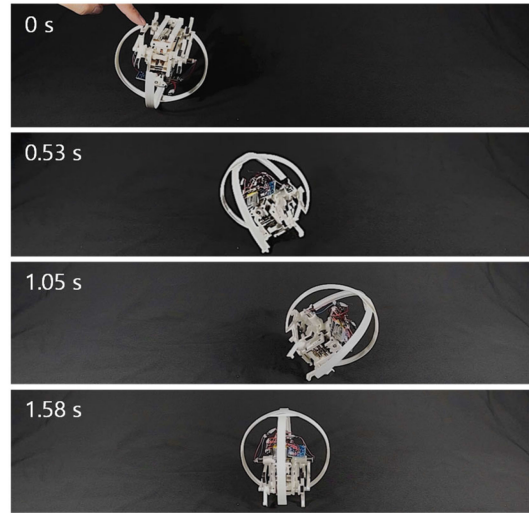


Fig. 5. Snapshot of the self-righting procedure of the robot. The robot can passively correct its posture by using the self-righting shell.

on each side of the body are connected to a motor by a gear transmission (reduction ratio of 64:1) and actuated simultaneously. By independently actuating the motor on each side of the body, the robot can change its crawling direction. Since the jumping mechanism and the crawling mechanism share the same body, the overall mass of the robot is reduced.

E. Self-Righting Shell

Because of the rotation during jumping or the landing impact, the robot can land on the ground in a flipped posture. To correct a posture, the passive self-righting shell (length of 155 mm, width of 125 mm, and height of 125 mm) was installed on the robot. The shape of the shell was designed for the robot to have a higher center of mass (CoM) when the robot is in the flipped posture than when it is in the correct posture. Therefore, the robot is able to roll from any flipped posture and can self-right to be stabilized at the lowest gravitational potential energy. The robot takes a few seconds to passively self-right its posture after jumping (see Fig. 5). In addition, the self-righting shell reduces the impact force of the collision during landing, protecting the robot.

F. Implementation of the Robot

All of the mechanisms mentioned above and the electronic components are integrated into a single robot (see Fig. 1). The mass budget of the robot is shown in Table II, which consists of two springs (advantage rubber band #64, Alliance), 3D-printed components, including the jumping linkage, body frame, and self-righting shell (ABSplus, uPrint SE Plus, Stratasys), a jumping motor (1000:1 geared dc motor, Pololu), two crawling motors (coreless dc motor, MK07-1.7, Didel), gears of the crawling transmission (pinion gear, G312-078, spur gear, G348L, Didel), electronics including a controller (CurieNano, DFRobot) and two motor drivers (HR8833, DFRobot), and a battery(Lithium-Polymer, 220 mAh, 15C). The average power consumption of

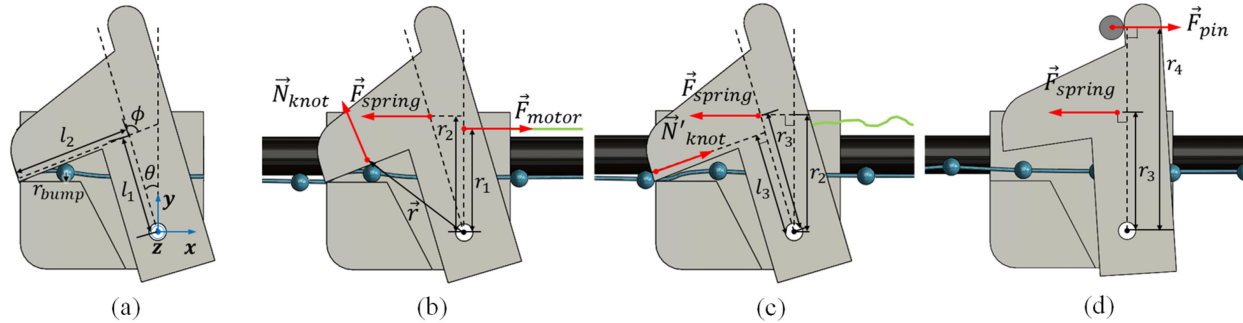


Fig. 6. Static model of the spring-linkage decoupling clutch. (a) Coordinate and geometric variables of the claws. Applied force when (b) storing energy, (c) releasing energy, (d) recovering the linkage, which is related to the equation of motion of the x -direction and z -direction.

TABLE II
MASS BUDGET

Components	Mass (g)
Spring (2 ea)	2.6
Jumping linkage	8.2
Jumping motor	11.5
Body frame	31.1
Crawling motor (2 ea)	5.6
Crawling transmission	14.3
Self-righting shell	10.8
Electronics	15.0
Battery (220 mAh, 15 C)	5.5
Total	104.6

the robot is about 3.4 W (0.4 W for the controller, 2.5 W for crawling, and 0.5 W for jumping), so the robot can operate for about 16 min. The robot is remotely controlled by Bluetooth communication between the computer and the robot.

III. MODELING

Two analytic models were examined: a static model for determining the geometric parameters of the spring-linkage decoupling clutch, and a dynamic model for predicting the jumping performance depending on the amount of energy storage.

A. Static Model of the Spring-Linkage Decoupling Clutch

The spring-linkage decoupling clutch has to perform the following three functions: opening the claws when storing the energy to disconnect the spring and the jumping linkage, closing the claws when releasing the energy to connect the spring and the linkage, and opening the claws after releasing the energy to disconnect again. To passively perform these functions, the geometry of the clutch, which affects the net torque applied to the claw, has to be well-tuned. Thus, we proposed a quasi-static model of the clutch to determine the design parameters of the clutch. Applied forces and geometric variables of the spring anchor for each situation are shown in Fig. 6. It is assumed that the spring anchor has quasi-static movement during storing and releasing the energy, satisfying the force equilibrium.

When storing the energy, the claws are closed until the spring anchor touches the knot. The force equilibrium and moment

inequality are as follows:

$$\sum F_x = F_{\text{motor}} - F_{\text{spring}} = 0 \quad (1)$$

$$\sum M_z = r_2 F_{\text{spring}} - r_1 F_{\text{motor}} > 0 \quad (2)$$

$$r_2 > r_1 \quad (3)$$

where r_1 and r_2 are the length of the moment arms of the spring and motor wire about the rotation axis of the rotational claw, respectively.

When a knot is in contact with the rotational claw, the claws have to be opened to pass by the knot [see Fig. 6(b)]. The force equilibrium and moment inequality are as follows:

$$\sum F_x = F_{\text{motor}} - N_{\text{knot}} \sin \theta - F_{\text{spring}} = 0 \quad (4)$$

$$\sum M_z = r_2 F_{\text{spring}} + \tau_{\text{knot}} - r_1 F_{\text{motor}} < 0 \quad (5)$$

$$\tau_{\text{knot}} = \vec{r} \times \vec{N}_{\text{knot}} \quad (6)$$

$$\vec{r} = \begin{bmatrix} -l_1 \sin \theta - \left(l_2 - \frac{r_{\text{knot}}}{\tan(\frac{\pi}{4} - \frac{(\phi - \theta)}{2})} \right) \sin(\phi - \theta) \\ l_1 \cos \theta - \left(l_2 - \frac{r_{\text{knot}}}{\tan(\frac{\pi}{4} - \frac{(\phi - \theta)}{2})} \right) \cos(\phi - \theta) \end{bmatrix} \quad (7)$$

$$\vec{N}_{\text{knot}} = \begin{bmatrix} -N_{\text{knot}} \sin(\frac{\pi}{2} - (\phi - \theta)) \\ N_{\text{knot}} \cos(\frac{\pi}{2} - (\phi - \theta)) \end{bmatrix} \quad (8)$$

where N_{knot} is the magnitude of the normal force of the knot, ϕ is the hook angle of the rotational claw, θ is the closed angle of the claw with respect to the y -axis, l_1 and l_2 are the geometric length of the rotational claw, and r_{bump} is the radius of the knot. By using (4) and (6), inequality (5) is simplified as follows:

$$F_{\text{spring}} \left(r_2 + \frac{\alpha}{\sin \theta} \right) < F_{\text{motor}} \left(r_1 + \frac{\alpha}{\sin \theta} \right) \\ \left(\alpha = l_2 - \frac{r_{\text{knot}}}{\tan(\frac{\pi}{4} - \frac{\phi - \theta}{2})} - l_1 \cos \phi \right) \quad (9)$$

If we assume that the term $(r_2 + \frac{\alpha}{\sin \theta})$ is negative, inequality (9) is simplified with inequality (3), as follows:

$$F_{\text{spring}} > F_{\text{spring}} \left(\frac{r_2 + \frac{\alpha}{\sin \theta}}{r_1 + \frac{\alpha}{\sin \theta}} \right) > F_{\text{motor}} \quad (10)$$

From (4), N_{knot} should be positive, and it requires F_{motor} to be larger than F_{spring}

$$N_{\text{knot}} = \frac{F_{\text{spring}} - F_{\text{motor}}}{\sin\theta} \geq 0 \quad (11)$$

$$F_{\text{spring}} \leq F_{\text{motor}} \quad (12)$$

Inequality (10) contradicts inequality (12). Thus, the term $(r_2 + \frac{\alpha}{\sin\theta})$ should be positive, and inequality (9) is simplified as follows:

$$r_2 \sin\theta + l_2 - \frac{r_{\text{knot}}}{\tan\left(\frac{\pi}{4} - \frac{\phi-\theta}{2}\right)} - l_1 \cos\phi > 0 \quad (13)$$

To simplify inequality (13), we set the parameter $\phi = \frac{\pi}{2}$, so inequality (13) is simplified as follows:

$$r_{\text{knot}} < (l_2 + r_2 \sin\theta) \tan\frac{\theta}{2} \quad (14)$$

Following inequality (14), the diameter of the knot should be smaller than 2.7 mm with the geometrically constrained parameters ($l_2 = 6$ mm, $r_2 = 5$ mm, $\theta_0 = 20^\circ$). The knotted string with target knot radius was manually fabricated. To check the consistency of the geometry, we fabricated 70 samples of knotted string and measured the diameter of a knot and the distance between knots; results show that the average diameter of a knot is 1.32 mm (standard deviation of 0.08) and the average distance between the knots is 6.02 mm (standard deviation of 0.35).

Also, inequality (9) is simplified as follows:

$$F_{\text{spring}} \left(\frac{r_2 + \frac{\alpha}{\sin\theta}}{r_1 + \frac{\alpha}{\sin\theta}} \right) < F_{\text{motor}}. \quad (15)$$

Inequality (15) suggests the required loading force of the motor to stretch the spring. To minimize the required loading force of the motor with the constraint (3), we selected r_1 and r_2 with similar values; the spring and the motor wire are anchored to the rotational claw with a similar location ($r_1 = 4.7$ mm, $r_2 = 5$ mm) relative to the rotation axis.

When releasing the energy, the tension of the wire disappears and a knot is in contact with the rotational claw in the opposite direction, as compared to the energy storing case [see Fig. 6(c)]. The claws should be closed to clamp the knot, which is determined by the force equilibrium and moment inequality, as follows:

$$\sum F_x = N'_{\text{knot}} \cos\theta_0 - F_{\text{spring}} = 0 \quad (16)$$

$$\sum M_z = r_2 F_{\text{spring}} - l_3 N'_{\text{knot}} > 0 \quad (17)$$

$$r_2 \cos\theta_0 > l_3. \quad (18)$$

After releasing the energy, the claws have to be opened again [see Fig. 6(d)]. The decoupling pin in contact with the upper part of the rotational claw generates the opening torque of the claws. The force equilibrium and moment inequality are as follows:

$$\sum F_x = F_{\text{pin}} - F_{\text{spring}} = 0 \quad (19)$$

$$\sum M_z = r_3 F_{\text{spring}} - r_4 F_{\text{pin}} > 0 \quad (20)$$

$$r_3 = \frac{r_2}{\cos\theta} < r_4. \quad (21)$$

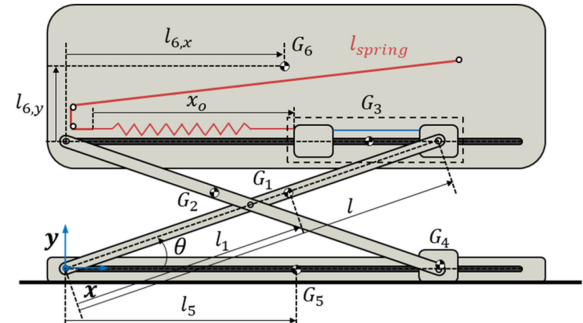


Fig. 7. Dynamic model of the robot during jumping. The robot consists of six links, with 1 degree of freedom. The CoM of each link is G_i , and the general coordinate is θ .

The length of the moment arm of the tip of the claw (l_3) and decoupling pin (r_4) is designed to be 3.4 mm and 9.4 mm to satisfy inequalities (18) and (21). The results of the static model were indirectly verified in the experiment, showing that the clutch works properly for each state, in the results section.

B. Dynamic Model of Jumping

To jump to the desired height, it is necessary to predict the jumping height of the robot depending on the amount of energy storage in the spring (i.e., spring displacement). In a ballistic motion, jumping height is determined by the take-off velocity. We used a Lagrangian dynamics model to investigate the jumping motion and obtained the take-off velocity. The kinematic coordinates of the jumping mechanism are simply represented in Fig. 7, consisting of six links with one degree of freedom. In this model, a single generalized coordinate (θ), which is the angle between links 1 and 5, was used. Following are the position and rotation vectors of the CoM of each link:

$$\vec{G}_1 = [l_1 \cos\theta; l_1 \sin\theta] \quad (22)$$

$$\vec{G}_2 = [(l - l_1) \cos\theta; l_1 \sin\theta] \quad (23)$$

$$\vec{G}_3 = [l \cos\theta - \alpha_3 (l \cos\theta_0 - x_0); l \sin\theta] \quad (24)$$

$$\vec{G}_4 = [(l - l_1) \cos\theta; l_1 \sin\theta] \quad (25)$$

$$\vec{G}_5 = [l_5; 0] \quad (26)$$

$$\vec{G}_6 = [l_{6,x}; l \sin\theta + l_{6,y}] \quad (27)$$

$$[\vec{R}_1; \vec{R}_2; \vec{R}_3; \vec{R}_4; \vec{R}_5; \vec{R}_6] = [\theta; -\theta; 0; 0; 0; 0] \quad (28)$$

where l is the length of the crossing link, θ_0 is the initial value of the generalized coordinate, x_0 is the spring displacement, which determines the amount of the energy storage, and $l_i, l_{i,x}, l_{i,y}$ are the distance from the far end to the CoM of each link, respectively. Since the spring anchor and the slider link are connected and move together during jumping, we considered the spring anchor and slider link as a single body (link 3). Thus, \vec{G}_3 is a position vector of the CoM of the spring anchor and slider link, and α_3 is the ratio of the mass of the spring anchor to the slider link.

The kinetic energy and potential energy are derived by position, rotation vectors, and its derivatives. Using kinetic and potential energy, the equation of motion described in general coordinate θ is derived from the Euler–Lagrange equation, as follows:

$$\begin{aligned} & (m_1 l_1^2 + m_2 l_2^2 + (m_3 + m_4 \sin^2 \theta + m_6 \cos^2 \theta)l + I_1 + I_2) \ddot{\theta} \\ &= k(l_{\text{prestr}} - l_{\text{nat}} + x_0 - (l \cos \theta_0 - l \cos \theta)) \\ &\quad - (m_4 l^2 - m_6 l^2) \sin \theta \cos \theta \dot{\theta}^2 \\ &\quad - (m_1 g l_1 + m_2 g l_2 + m_3 g l + m_6 g l) \cos \theta \end{aligned} \quad (29)$$

where m_i is the mass of each link, I_i is the moment of inertia of each link, k is the stiffness of the spring, l_{nat} and l_{prestr} are the natural and prestretched length of the spring, respectively. The differential equation is numerically solved by using MATLAB. We treated that the robot takes off from the ground when the vertical GRF becomes zero, and obtained a take-off velocity. Using this velocity, we calculated the jumping heights of the robot by energy conservation law. As a result of the dynamic model, we predicted the jumping heights of the robot depending on the spring displacements. The results of the modeling were presented and compared with the experimental results, in the next section.

IV. RESULTS

The following section describes the experiments evaluating the agility and energy-efficiency of the proposed jumping–crawling robot. First, to verify that the spring-linkage decoupling clutch works properly, we checked the working procedure of the clutch in energy storing and releasing process. By using the clutch, the jumping–crawling robot has two main functional improvements: rapid transition of locomotion and enhanced jumping height adjustment. We measured the transition duration from jumping to crawling to show the rapid transition of locomotion, and measured the jumping height depending on the spring displacement to show the enhanced jumping height adjustment. These features enable the jumping–crawling robot rapidly and energy-efficiently overcome various sizes of obstacles. To validate the enhanced performance, we conducted a demonstration of multimodal locomotion of the proposed robot and measured the time and energy consumption. The results were compared to the robot without the decoupling mechanism, to evaluate the enhancement of agility and energy-efficiency.

A. Decoupling Movement of the Linkage and the Spring

To verify the spring-linkage decoupling clutch working properly, we checked the working procedure of the clutch in energy storing and releasing process, and recorded the motion of the jumping linkage and the spring using a high-speed camera (Miro eX4, Phantom, 2000 fps) (see supplementary video and Fig. 8). When storing the energy (time during -27 – 0 s), the spring anchor (colored in blue) slowly moves from the left to the right side, and the jumping linkage (colored in red) maintains its position. This means that the spring can be deformed while maintaining a crouched jumping linkage. When releasing the

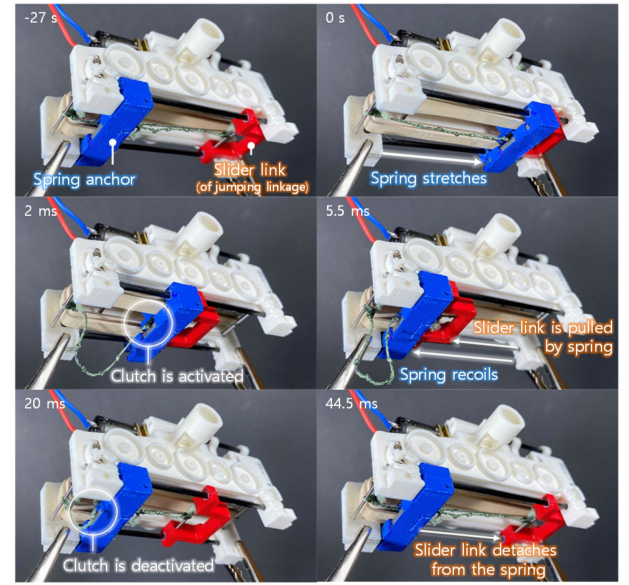


Fig. 8. Working procedure of the spring-linkage decoupling clutch in energy storing and releasing process. To show a clear view, pictures of the robot that stopped in an actual working timestamp were taken. The actual working procedure was recorded by a high-speed camera (available online as supplementary video).

energy (time 0–5.5 ms), the spring anchor rapidly moves to the left side; simultaneously, the jumping linkage moves together with the spring anchor. This means that the recoil force of the spring is transferred to the extending jumping linkage. After releasing the energy (time 5.5–44.5 ms), the transferred jumping linkage starts returning, while maintaining the position of the spring anchor. This means that the extended linkage can be crouched without storing energy. It takes about 39 ms to crouch the jumping linkage; this is shorter than the time for the robot to land on the ground after jumping. These results show that the spring-linkage decoupling clutch properly decouples the movement of the jumping linkage and the control of the energy storage.

B. Rapid Transition of Locomotion and Enhanced Jumping Height Adjustment

By integrating the spring-linkage decoupling clutch, the jumping–crawling robot can rapidly change its locomotion type and the adjustable range of the jumping height can be widened. First, to show the rapid transition of locomotion, we measured the transition duration from jumping to crawling of the proposed robot, and compared it to a robot without the spring-linkage decoupling clutch (i.e., the decoupling mechanism) (see the details in the supplementary video). The results show that the transition duration of the robot without the decoupling mechanism is longer than 30 s. This is because the energy also has to be stored in the spring when crouching the jumping linkage in order to start crawling. In contrast, the proposed robot rapidly crouches the jumping linkage and self-rights within 3 s after jumping. Second, to validate the performance of jumping height adjustment, we measured the jumping height of the robot depending on the

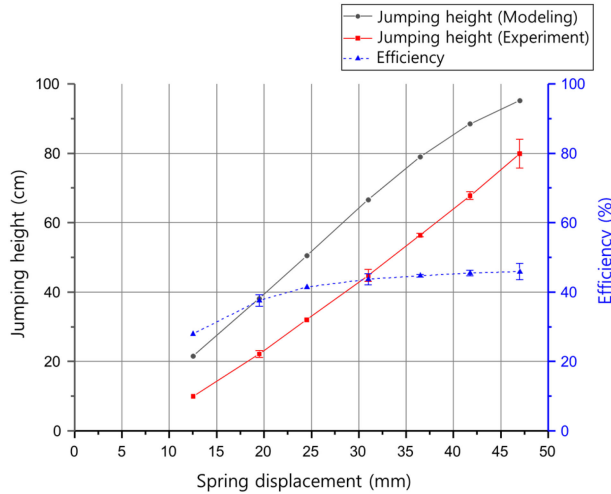


Fig. 9. Modeling and experimental results of the jumping height, and energy efficiency depending on the spring displacement. The red and blue solid markers denote the average of five trials, and the bars represent ± 1 standard deviation.

spring displacement, and compared it with the modeling results obtained from the previous section (Fig. 9, black and red lines). The spring displacement is adjusted in seven steps, and the robot repeatedly jumps five times for each step. Jumping height was measured by the displacement of the CoM of the robot. As a result, the jumping height linearly increased from 10 to 80 cm as the spring displacement increased. The spring-linkage decoupling clutch enables the robot to control a wide range of energy storage while maintaining the crouching jumping linkage. The modeling results predict the monotonic increase of jumping height depending on the spring displacement as well. However, the experimental results show 10 cm smaller than the modeling results at each spring displacement. This difference is due to energy losses not considered in the model, such as hysteresis of the spring or frictions of the jumping linkages. To validate how much energy losses during jumping, we calculated mechanical energy-efficiency (Fig. 9, blue line). Mechanical energy-efficiency was calculated as the ratio of the gravitational potential energy when a robot is at apex, to elastic energy stored in the spring. The efficiency increases from 28.0% to 45.9% as the spring displacement increases. It can be enhanced by reducing the friction of the jumping linkage, or reducing the rotation of the robot.

C. Agility and Energy-Efficiency of the Robot

As for robotic systems, Eckert and Ijspeert [43] defined agility as the ability to perform a series of different tasks executed in a fast and efficient manner. The main tasks of the jumping–crawling robot are to perform jumping and crawling locomotion to navigate various sizes of ground obstacles. Therefore, in this article, the agility of the jumping–crawling robot was considered as the ability to rapidly perform multimodal locomotion. From this point of view, the agility of the robot was quantitatively evaluated by measuring the time consumption accomplishing the multimodal locomotion. Similarly, energy-efficiency was

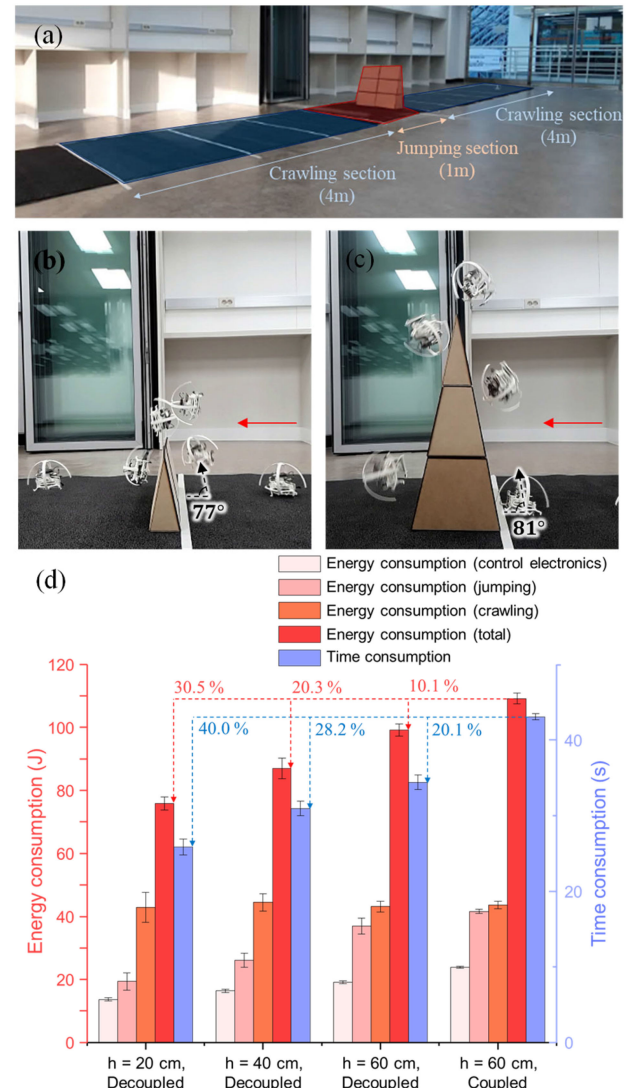


Fig. 10. (a) Ground track consisting of two crawling sections (4 m), and a jumping section (1 m) with different heights of hurdles (20, 40, and 60 cm). While the robot traversed the track, the time and energy consumption were measured. (b), (c) Snapshots of the robot traversing the track with different heights of hurdles [(b) for 20 cm, and (c) for 60 cm]. (d) Energy and time consumption of the robot for 4 cases. Bold red bar represents total energy consumption, and it breaks down into three categories: control electronics, jumping, and crawling. They are indicated by different red shades (represented in the upper label). Thick bars represent mean values, and thin bars represent ± 1 standard deviation.

evaluated by measuring energy consumption during multimodal locomotion. To evaluate agility and energy-efficiency, we tested the robot overcoming various sizes of obstacles by performing multimodal locomotion, and measured the time and energy consumption (see Fig. 10 and supplementary video). The robot traverses a specific ground track [see Fig. 10(a)], which consists of two crawling sections (length of 4 m) and a jumping section (length of 1 m) with different heights of hurdles. The robot approaches each hurdle by crawling, crosses over it by jumping, and goes further by crawling again, as shown in Fig. 10(b) and (c). The results show that the robot passes over different heights of hurdles with a fitted trajectory through the jumping height and

jumping angle adjustment. Jumping angle adjustment is also an important ability to change the horizontal displacement of the jumping. Previously developed jumping robots adjust jumping angles by adjusting the posture [44]. Differently, the proposed robot adjusts the launch angle, from 85.1° to 71.8° , by adjusting the crawling speed and take-off velocity.

The time consumption and energy consumption were measured in a total of four cases: three cases of the proposed robot with different obstacle heights (20, 40, and 60 cm), and one case of the robot without the decoupling mechanism with a fixed jumping height (60 cm) as a control group. Since the robot without the decoupling mechanism has a limited range of jumping height adjustment, just one jumping height case was tested. Each case was repeated five times. Energy consumption was calculated by the product of the voltage and current of the battery over time, which were measured by a current sensor (INA219, DFRobot). Fig. 10(d) plots the average time and energy consumption of the robot for each case. The results show, in the case of total time consumption (blue bar, right vertical axis), the robot without the decoupling mechanism consumes 43.0 s to travel the track, while the proposed robot consumes 25.8, 30.9, and 34.4 s, for the heights of 20 cm, 40 cm, and 60 cm, respectively. These results mean that the proposed robot reduces the time consumption of up to 40.0%, compared to the robot without the decoupling mechanism. In the case of total energy consumption (red bar, left vertical axis), the robot without the decoupling mechanism consumes 109.0 J to travel the track, while the proposed robot consumes 75.8, 87.0, and 99.1 J, for the height of 20 cm, 40 cm, and 60 cm, respectively. These results mean that the proposed robot can save energy of up to 30.5%, compared to the robot without the decoupling mechanism. To analyze in detail, specified energy consumptions of control electronics, jumping, and crawling were also plotted (indicated by different red shades bars). Since crawling distance in each test case varies little, energy consumption of crawling also shows not much of a difference between the proposed robot (42.9, 44.4, and 43.1 J for the height of 20 cm, 40 cm, and 60 cm, respectively) and the robot without the decoupling mechanism (43.6 J). The proposed robot reduces the completion time through the rapid transition of locomotion, and the completion time proportionally increases the energy consumption of the electronics. Therefore, the proposed robot shows less energy consumption on control electronics (13.7, 16.4, and 19.1 J for the height of 20 cm, 40 cm, and 60 cm, respectively) than the robot without decoupling mechanism (23.9 J). Since higher jump requires more energy, the proposed robot which performs fitted jumping shows less energy consumption on jumping (19.3, 26.1, and 36.9 J for the height of 20 cm, 40 cm, and 60 cm, respectively) than the robot without the decoupling mechanism (41.6 J). The rapid transition of locomotion and enhanced jumping height adjustment enable the proposed robot performs multimodal locomotion with reduced time and energy consumption, enhancing its agility and energy-efficiency.

D. Field Demonstrations—Classroom Navigation

To show an application of the proposed robot, we performed a classroom navigation test (see Fig. 11, and supplementary

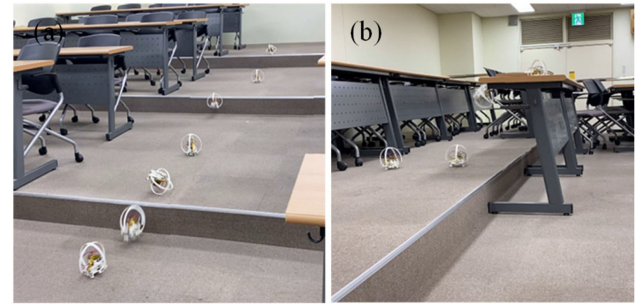


Fig. 11. Snapshots of the robot navigating a university classroom. (a) Leaping up multiple stairs by repeated low jumping and crawling. (b) Leaping up on a desk by high jumping.

video). In a university classroom, various sizes of objects such as stairs, chairs, and desks were densely placed. The robot successfully and rapidly leaped up the multiple steps of a stair with repeated low jumping and crawling [see Fig. 11(a)], and leaped up on a desk with high jumping [see Fig. 11(b)].

V. CONCLUSION

In this article, we presented an agile and energy-efficient jumping–crawling robot through the rapid transition of locomotion and enhanced jumping height adjustment. These advances are achieved by decoupling the transition of locomotion and control of the energy storage of the robot, which were previously coupled by the movement of the jumping linkage. To decouple two functions, we designed the spring-linkage decoupling clutch, which can properly switch the connection between the jumping linkage and the spring. Using the static model, we characterized the spring-linkage decoupling clutch and then determined the design parameters for robust clutching. By using the clutch, the jumping–crawling robot can rapidly change its locomotion type and perform a wide range of jumping height adjustment. Both advancements were verified through experiments and analysis. From the dynamic model, we were able to predict and control the jumping height, depending on the spring displacement; this was also confirmed by the experimental results. We conducted a demonstration of multimodal locomotion which validates the reduction of the time and energy consumption of the jumping–crawling robot up to 40% and 30%, respectively, compared to the robot without the proposed decoupling mechanism. This result shows our decoupling approach is feasible for increasing the agility and energy-efficiency of a jumping–crawling robot, and this approach can be applied to different types of jumping–crawling robots that use parallel elastic systems for power amplification.

In order to utilize the proposed robot in a real task, such as exploration or rescue missions, several further developments have to be accomplished. During navigation, the robot will encounter various terrains, which could affect the locomotion performance. To predict and control the movement of the robot at different terrains, studies on the effect of surface types on jumping are required. We performed a preliminary test measuring the jumping height of the robot on different surfaces, such as carpet or slippery surface, which were utilized in the experiments of this article. The results show the ignorable differences in

jumping heights between our tested surfaces. However, this test was performed on very limited surfaces and further investigation is required. The jumping is obviously affected by the mechanical characteristics of the ground material. For instance, stiffness of the surface affects the take-off timing when jumping, which may cause the robot prematurely takes off from the ground before all the stored energy is released. Also, damping effect of a surface such as granular media dissipates the kinetic energy of the robot during jumping.

Also, in order to expand the operating time, energy-efficiency of the jumping locomotion has to be further improved. In this article, we showed that our approach which decouples energy storage and the movement of the jumping linkage enhances the energy-efficiency of the jumping–crawling robot. However, designing kinematics of a jumping transmission to improve mechanical energy-efficiency was not dealt with. Kinematics of a linkage transmission affects the GRF profile, which may cause unwanted motion, such as rotation or prematurely take-off as mentioned above. In addition, the electrical energy-efficiency of the actuator also should be enhanced. For a centimeter-scale jumping robot that utilizes the spring to amplify an actuator's limited power, an actuator slowly deforms the spring by a large torque, which is generated by a high current and high gear reduction ratio; both are very inefficient ways of use. The electrical energy-efficiency of the actuator of the proposed robot is about 4%. To increase the energy-efficiency, the characteristics of the actuator, spring, and transmission should be optimized.

Finally, the productivity of the robot should also be considered. The proposed robot was just developed and tested in a laboratory; most of the components of the robot are 3-D printed and manually assembled, increasing the production time and price. In order to increase productivity, mass production of the components and production automation are necessary. For example, 3-D printing of parts can be replaced with the injection molding of plastic materials, which reduces the fabrication time and cost. Also, the design of the robot can be optimized to reduce the number of components, which reduces the assembly time.

REFERENCES

- [1] R. M. Alexander, *Principles of Animal Locomotion*. Princeton, NJ, USA: Princeton Univ. Press, 2003.
- [2] U. Saranli, M. Buehler, and D. E. Koditschek, “RHex: A simple and highly mobile hexapod robot,” *Int. J. Robot. Res.*, vol. 20, no. 7, pp. 616–631, 2002.
- [3] S. Kim, J. E. Clark, and M. R. Cutkosky, “iSprawl: Design and tuning for High-speed autonomous Open-loop running,” *Int. J. Robot. Res.*, vol. 25, no. 9, pp. 903–912, 2006.
- [4] A. M. Hoover, E. Steltz, and R. S. Fearing, “RoACH: An autonomous 2.4g crawling hexapod robot,” in *Proc. IEEE Int. Conf. Intell. Robots Syst.*, 2008, pp. 26–33.
- [5] P. Birkmeyer, K. Peterson, and R. S. Fearing, “DASH: A dynamic 16g hexapod robot,” in *Proc. IEEE/RSJ Int. Conf. Intell. Robots Syst.*, 2009, pp. 2683–2689.
- [6] A. T. Baisch, C. Heimlich, M. Karpelson, and R. J. Wood, “HAMR3: An autonomous 1.7g ambulatory robot,” in *Proc. IEEE Int. Conf. Intell. Robots Syst.*, 2011, pp. 5073–5079.
- [7] D. W. Haldane, K. C. Peterson, F. L. G. Bermudez, and R. S. Fearing, “Animal-inspired design and aerodynamic stabilization of a hexapedal millirobot,” in *Proc. IEEE Int. Conf. Robot. Autom.*, 2013, pp. 3279–3286.
- [8] D. Zarrouk, A. Pullin, N. Kohut, and R. S. Fearing, “STAR, a sprawl tuned autonomous robot,” in *Proc. IEEE Int. Conf. Robot. Autom.*, 2013, pp. 20–25.
- [9] K. Jayaram and R. J. Full, “Cockroaches traverse crevices, crawl rapidly in confined spaces, and inspire a soft, legged robot,” *Proc. Nat. Acad. Sci. USA*, vol. 113, no. 8, pp. E950–E957, 2016.
- [10] T. Kim, C. Kim, S. Kim, and G. Jung, “MutBug: A lightweight and compact crawling robot that can run on both sides,” *IEEE Robot. Autom. Lett.*, vol. 4, no. 2, pp. 1409–1415, Apr. 2019.
- [11] J. Lee *et al.*, “CaseCrawler: A lightweight and low-profile crawling phone case robot,” *IEEE Robot. Autom. Lett.*, vol. 5, no. 4, pp. 5858–5865, Oct. 2020.
- [12] Y. Lee, D. Yoon, J. Oh, H. S. Kim, and T. Seo, “Novel angled spoke-based mobile robot design for agile locomotion with obstacle-overcoming capability,” *IEEE/ASME Trans. Mechatronics*, vol. 25, no. 4, pp. 1980–1989, Aug. 2020.
- [13] Y. Kim, Y. Lee, S. Lee, J. Kim, H. S. Kim, and T. Seo, “STEP: A new mobile platform with 2-DOF transformable wheels for service robots,” *IEEE/ASME Trans. Mechatronics*, vol. 25, no. 4, pp. 1859–1868, Aug. 2020.
- [14] S. Kim, M. Spenko, S. Trujillo, B. Heyneman, V. Mattoli, and M. R. Cutkosky, “Whole body adhesion: Hierarchical, directional and distributed control of adhesive forces for a climbing robot,” in *Proc. IEEE Int. Conf. Robot. Autom.*, 2007, pp. 1268–1273.
- [15] M. J. Spenko, G. C. Haynes, J. A. Saunders, M. R. Cutkosky, A. A. Rizzi, and R. J. Full, “Biologically inspired climbing with a hexapedal robot,” *J. Field Robot.*, vol. 25, no. 4/5, pp. 223–242, 2008.
- [16] U. Scarfogliero, C. Stefanini, and P. Dario, “Design and development of the long-jumping ‘Grillo’ mini robot,” in *Proc. IEEE Int. Conf. Robot. Autom.*, 2007, pp. 467–472.
- [17] M. Kovac, M. Fuchs, A. Guignard, J. Zufferey, and D. Floreano, “A miniature 7G jumping robot,” in *Proc. IEEE Int. Conf. Robot. Autom.*, 2008, pp. 373–378.
- [18] M. Noh, S. Kim, S. An, J. Koh, and K. Cho, “Flea-Inspired catapult mechanism for miniature jumping robots,” *IEEE Trans. Robot.*, vol. 28, no. 5, pp. 1007–1018, Oct. 2012.
- [19] D. W. Haldane, M. M. Plecnik, J. K. Yim, and R. S. Fearing, “Robotic vertical jumping agility via series-elastic power modulation,” *Sci. Robot.*, vol. 1, no. 1, 2016, Art. no. eaag2048.
- [20] G. C. H. E. D. Croon, K. M. E. D. Clercq, R. Ruijsink, B. Remes, and C. D. Wagter, “Design, aerodynamics, and vision-based control of the delfly,” *Int. J. Micro Air Veh.*, vol. 1, no. 2, pp. 71–97, 2009.
- [21] K. Y. Ma, P. Chirarattananon, S. B. Fuller, and R. J. Wood, “Controlled flight of a biologically inspired, insect-scale robot,” *Science*, vol. 340, no. 6132, pp. 603–607, 2013.
- [22] A. Ramezani, S.-J. Chung, and S. Hutchinson, “A biomimetic robotic platform to study flight specializations of bats,” *Sci. Robot.*, vol. 2, no. 3, 2017, Art. no. eaal2505.
- [23] Y. Chen *et al.*, “Controlled flight of a microrobot powered by soft artificial muscles,” *Nature*, vol. 575, no. 7782, pp. 324–329, 2019.
- [24] H. V. Phan, S. Aurecianus, T. Kang, and H. C. Park, “KUBeetle-S: An insect-like, tailless, hover-capable robot that can fly with a low-torque control mechanism,” *Int. J. Micro Air Veh.*, vol. 11, pp. 1–10, 2019.
- [25] Y. Sun *et al.*, “Soft mobile robots: A review of soft robotic locomotion modes,” *Curr. Robot. Rep.*, vol. 2, pp. 371–397, 2021.
- [26] S. A. Stoeter and N. Papanikolopoulos, “Kinematic motion model for jumping scout robots,” *IEEE Trans. Robot.*, vol. 22, no. 2, pp. 397–402, Apr. 2006.
- [27] B. G. Lambrecht, A. D. Horchler, and R. D. Quinn, “A small, insect-inspired robot that runs and jumps,” in *Proc. IEEE Int. Conf. Robot. Autom.*, 2005, pp. 1240–1245.
- [28] G. Jung *et al.*, “JumpRoACH: A trajectory-adjustable integrated jumping–crawling robot,” *IEEE/ASME Trans. Mechatronics*, vol. 24, no. 3, pp. 947–958, Jun. 2019.
- [29] J. Zhang, G. Song, G. Qiao, Z. Li, W. Wang, and A. Song, “A novel one-motor driven robot that jumps and walks,” in *Proc. IEEE Int. Conf. Robot. Autom.*, 2013, pp. 13–19.
- [30] T. Mao, H. Peng, X. Lu, and C. Zhao, “A small locust inspired actuator driven by shape memory alloys and piezoelectric strips,” *Smart Mater. Structures*, vol. 28, no. 10, 2019, Art. no. 105051.
- [31] J. Zhao, W. Yan, N. Xi, M. W. Mutka, and L. Xiao, “A miniature 25 grams running and jumping robot,” in *Proc. IEEE Int. Conf. Robot. Autom.*, 2014, pp. 5115–5120.
- [32] G. Song, K. Yin, Y. Zhou, and X. Cheng, “A surveillance robot with hopping capabilities for home security,” *IEEE Trans. Consum. Electron.*, vol. 55, no. 4, pp. 2034–2039, Nov. 2009.

- [33] N. Meiri and D. Zarrouk, "Flying STAR, a hybrid crawling and flying sprawl tuned robot," in *Proc. IEEE Int. Conf. Robot. Autom.*, 2019, pp. 5302–5308.
- [34] Y. Mulgaonkar *et al.*, "The flying monkey: A mesoscale robot that can run, fly, and grasp," in *Proc. IEEE Int. Conf. Robot. Autom.*, 2016, pp. 4672–4679.
- [35] S.-M. Baek, S. Yim, S.-H. Chae, D.-Y. Lee, and K.-J. Cho, "Ladybird beetle-inspired compliant origami," *Sci. Robot.*, vol. 5, 2020, Art. no. 41.
- [36] M. A. Woodward and M. Sitti, "Multimo-Bat: A biologically inspired integrated jumping–gliding robot," *Int. J. Robot. Res.*, vol. 33, no. 12, pp. 1511–1529, 2014.
- [37] M. Kovac, W. Hraiz, O. Fauria, J. Zufferey, and D. Floreano, "The EPFL jumpglider: A hybrid jumping and gliding robot with rigid or folding wings," in *Proc. IEEE/RSJ Int. Conf. Robot. Biomimetics*, 2011, pp. 1503–1508.
- [38] M. T. Pope *et al.*, "A multimodal robot for perching and climbing on vertical outdoor surfaces," *IEEE Trans. Robot.*, vol. 33, no. 1, pp. 38–48, Feb. 2017.
- [39] R. J. Lock, S. C. Burgess, and R. Vaidyanathan, "Multi-modal locomotion: From animal to application," *Bioinspiration Biomimetics*, vol. 9, no. 1, 2013, Art. no. 011001.
- [40] M. Ilton *et al.*, "The principles of cascading power limits in small, fast biological and engineered systems," *Science*, vol. 360, 2018, Art. no. 6387.
- [41] M. F. Ashby, *Materials Selection in Mechanical Design*. Princeton, NJ, USA: Princeton Univ. Press, 2003.
- [42] S. E. Bergbreiter, "Autonomous jumping microrobots," Ph.D. dissertation, Dept. Electrical Engineering and Computer Science, Univ. of California, Berkeley, USA, 2007.
- [43] P. Eckert and A. J. Ijspeert, "Benchmarking agility for multilegged terrestrial robots," *IEEE Trans. Robot.*, vol. 35, no. 2, pp. 529–535, Apr. 2019.
- [44] J. Zhang, G. Song, Z. Li, G. Qiao, H. Sun, and A. Song, "Self-Righting, steering and takeoff angle adjusting for a jumping robot," in *Proc. IEEE Int. Conf. Intell. Robots Syst.*, 2012, pp. 2089–2094.



Soo-Hwan Chae (Student Member, IEEE) received the B.S. degree in mechanical and aerospace engineering from Seoul National University, Seoul, South Korea, in 2017, where he is currently working toward the Ph.D. degree in mechanical engineering with the Biorobotics Laboratory.

His current research interests include the design and fabrication of biologically inspired robots.



Sang-Min Baek received the B.S. degree in mechanical engineering from the Korea Advanced Institute of Science and Technology, Daejeon, South Korea, in 2014. He is currently working toward the Ph.D. degree in mechanical engineering with the Biorobotics Laboratory, Seoul National University, Seoul, South Korea.

His current research interests include the design and fabrication of biologically inspired robots.



Jongeun Lee received the B.S. degree in mechanical and aerospace engineering from Seoul National University, Seoul, South Korea, in 2016. He is currently working toward the Ph.D. degree in mechanical engineering with the Biorobotics Laboratory, Seoul National University, Seoul, South Korea.

His current research interests include the design and fabrication of biologically inspired robots.



Kyu-Jin Cho (Member, IEEE) received the B.S. and M.S. degrees in mechanical engineering from Seoul National University, Seoul, South Korea, in 1998 and 2000, respectively, and the Ph.D. degree in mechanical engineering from the Massachusetts Institute of Technology, Cambridge, MA, USA, in 2007.

He was a Postdoctoral Fellow with Harvard Microrobotics Laboratory until 2008. He is currently an Associate Professor of Mechanical and Aerospace Engineering and the Director of Biorobotics Laboratory, Seoul National University. His research interests include biologically inspired robotics, soft robotics, soft wearable robots, and rehabilitation/ assistive robotics.

Dr. Cho was the recipient of the 2014 IEEE RAS Early Academic Career Award, 2014 ASME Compliant Mechanism Award, and 2013 IROS Best Video Award.